ISBN 978-90-481-2696-5

NATO Science for Peace and Security Series - C:
Environmental Security

Coupled Site and Soil-Structure Interaction Effects with Application to Seismic Risk Mitigation

Edited by
Tom Schanz
Roumen Iankov

SOIL-STRUCTURE INTERACTION IN NONLINEAR SOIL

Vlado Gicev (vgicev@gmail.com)
Department of Computer Science,
Goce Delcev University, Toso Arsov St. 14, 2000 Stip,
F.Y.R. of Macedonia

Abstract. A two-dimensional (2-D) model of a building supported by a semi-circular flexible foundation embedded in nonlinear soil is analyzed. The building, the foundation, and the soil have different physical properties. The model is excited by a half-sine SH wave pulse, which travels toward the foundation. The results show that the spatial distribution of permanent, nonlinear strain in the soil depends upon the incident angle, the amplitude, and the duration of the pulse. If the wave has a large amplitude and a short duration, a nonlinear zone in the soil appears immediately after the reflection from the half-space and is located close to the free surface. This results from interference of the reflected pulse from the free surface and the incoming part of the pulse that still has not reached the free surface. When the wave reaches the foundation, it is divided on two parts—the first part is reflected, and the second part enters the foundation. Further, there is separation of this second part at the foundation-building contact. One part is reflected back, and one part enters the building. After each contact of the part of the wave that enters the building with the foundation-building contact, one part of the wave energy is released back into the soil. This process continues until all of the energy in the building is released back into the soil. The work needed for the development of nonlinear strains spends part of the input wave energy, and thus a smaller amount of energy is available for exciting the building.

Keywords: soil-structure interaction; non-linear wave propagation; energy distribution

1. Introduction

Field reconnaissance of the effects of many earthquakes has provided numerous examples of different types of soil failure and permanent deformations caused by strong shaking. Examples include settlement of cohesionless soils, liquefaction of saturated sands, flow slides due to liquefaction of cohesionless soils, bulkhead failures due to backfill liquefaction, slides caused by liquefaction of thin sand layers, failures of fills on weak foundations, and lateral movement of bridge abutments. Many structures settle, tilt, or overturn on liquefied soil. Some of the best-known examples of this occurred during the 1964 Alaska and 1964 Niigata earthquakes (Seed, 1970). The sequence of the

T. Schanz and R. Iankov (eds.), *Coupled Site and Soil-Structure Interaction Effects with Application to Seismic Risk Mitigation,* NATO Science for Peace and Security Series C: Environmental Security,

soil-structure interaction (SSI) phenomena, which led to the overturning of apartment buildings in Kawagishi-cho during the Niigata earthquake, is complicated, and its complete modelling and analysis are still a major challenge for any nonlinear numerical simulation. It probably started with development of nonlinear strain zones in the soil close to the foundation, which in turn expanded the trapped nonlinear energy to initiate liquefaction. We are assuming here that the large energy of earthquake waves trapped in the zones of strain localization initiated liquefaction (Trifunac, 1995), which then spread all around the foundation, causing the buildings to tilt and overturn. Analysis of this sequence is well beyond the scope of this paper, however. We will describe only the early stages, which involve the creation of the nonlinear zones of soil response.

Trifunac (1972) presented the analytical solution for interaction of the wall sitting on an embedded semi-circular rigid foundation. Wong and Trifunac (1975) studied the wall–soil–wall interaction with the presence of two or more shear walls, and Abdel-Ghaffar and Trifunac (1977) studied the soil–bridge interaction with a semi-cylindrical rigid foundation and an input plane-SH wave. Other studies have been conducted to analyze the influence of the shape of a rigid foundation on the interaction. Wong and Trifunac (1974) solved the interaction of the shear wall erected on an elliptical rigid foundation for shallow and deep embedment, and Westermo and Wong (1977) studied different boundary models for the soil-structure interaction of an embedded, semi-circular, rigid foundation. They concluded that without a transmitting boundary all of the models develop resonant behaviour and that the introduced damping in the soil cannot adequately model the radiation damping. Luco and Wong (1977) studied a rectangular foundation welded to an elastic half-space and excited by a horizontally propagating Rayleigh wave. Lee (1979) solved a 3-D interaction problem consisting of a single mass supported by an embedded, hemispherical, rigid foundation for incident plane P, SV, and SH waves in spherical coordinates. The recent publications deal with a flexible foundation. Todorovska et al. (2001) solved an interaction of a dike on a flexible, embedded foundation, and Hayir et al. (2001) described the same dike but in the absence of a foundation. Aviles et al. (2002) analyzed the in-plane motion of a 4-degrees-of-freedom model and Gicev (2005) studied the soil-flexible foundation-structure interaction for incident-plane SH waves with a numerical model using finite differences.

The soil-structure interaction phenomenon includes several features, among them wave scattering, radiation damping, damping in the structure, and the presence of different frequencies (system frequency, apparent frequency, rocking frequency, horizontal frequency, and fixed-base frequency). In this paper, in the presence of the interaction, the development of the

nonlinear zones in the soil is studied for incident pulses representing the near-field destructive strong ground motion. The problems that must be addressed in the numerical study of the nonlinear soil-structure interaction include heterogeneities and discontinuities in the medium, the modelling of the free surface, artificial boundaries, and keeping track of the nonlinear constitutive law at each point in the soil. According to Moczo (1989) and Zahradnik et al. (1993), the computational FD schemes that are used in applications of wave propagation can be divided into homogenous and heterogeneous. Alterman and Karal (1968) used the homogeneous formulation to solve elastic wave propagation in layered media, and Boore (1972) proposed the heterogeneous scheme. Tsynkov (1998) reviewed the existing global and local artificial boundaries. The global boundaries are perfect absorbers, but they cannot be readily applied in "marching-in-time" procedures because of their non-locality, both in time and space. The main advantage of the local (imperfect) artificial boundaries is that they are local in space and time and are not frequency dependent.

2. Model

During the wave passage, the soil, the foundation, and the superstructure undergo nonlinear deformations and permanent strains. Because the aim of this paper is to study the nonlinear zones in the soil only—for simplicity—only the soil is modeled as nonlinear, while the foundation and the building are assumed to remain linear. The model is shown in Fig. 1. The incoming wave is a half-sine pulse of a plane SH wave. A dimensionless frequency

$$\eta = \frac{2a}{\lambda} = \frac{a}{\beta_s \cdot t_{d0}} \tag{1a}$$

is introduced as a measure of the pulse duration, where a is the radius of the foundation, λ is the wavelength of the incident wave, β_s is the shear-wave velocity in the soil, and t_{d0} is duration of the pulse.

To set up the grid spacing, the pulse is analysed in space domain (s), and the displacement in the points occupied by the pulse is

$$w(s) = A \sin \frac{\pi \cdot s}{\beta_s \cdot t_{d0}}, \tag{1}$$

where A is the amplitude of the pulse and s is the distance of the considered point to the wave front in initial time in the direction of propagation. Using the fast Fourier transform algorithm, the half-sine pulse Eq. (1) is transformed in wave number domain (k) as follows:

$$w(k) = \mathcal{F}(w(s)). \tag{2}$$

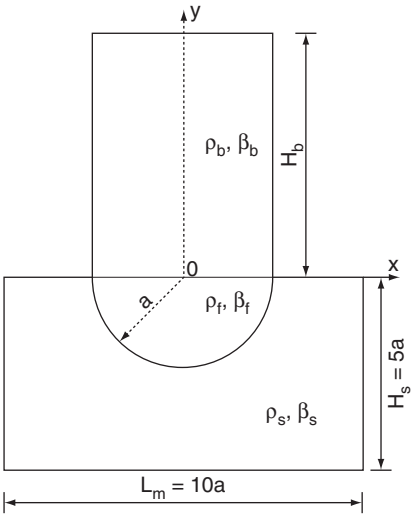

Figure 1. Soil-flexible foundation-structure system.

The maximum response occurs for $k = 0$ (rigid-body motion). As k increases, the response decreases and goes asymptotically to zero as k approaches infinity. We selected the largest wave number, $k = k_{\max}$, for which the k-response is at least 0.03 of the maximum response (dashed lines in Fig. 2a). Then, for this value of $k_{\max}$, the corresponding frequencies and the corresponding wavelengths are computed:

$$\lambda_{\min} = \frac{2\pi}{k_{\max}} = \frac{2\pi\beta}{\omega_{\max}}. \tag{3}$$

It can be seen from Fig. 2a that $\omega_{\max} \approx 245$ rad/s for $\eta = 0.5$, while $\omega_{\max} \approx 980$ rad/s for $\eta = 2$.

A measure of the numerical accuracy of the grid is related to the ratio between the numerical and physical velocity of propagation, $r = c/\beta$, which ideally should be 1. The parameters that influence this accuracy are:

- the density of the grid $m = \lambda/\Delta x$ (m is the number of points per wavelength λ and Δx is the spacing between the grid points);
- the Courant number, $\chi = \beta_s \Delta t/\Delta x$;
- the angle of the wave incidence, θ.

It has been shown (Alford et al., 1974; Dablain, 1986; Fah, 1992) that the error increases when m decreases, χ decreases, and θ is close to 0 or $\pi/2$. For second-order approximation, the above authors recommend $m = 12$.

To compare hysteretic energies and the nonlinear zones in the soil, the soil box should have the same dimensions for any dimensionless frequency of the

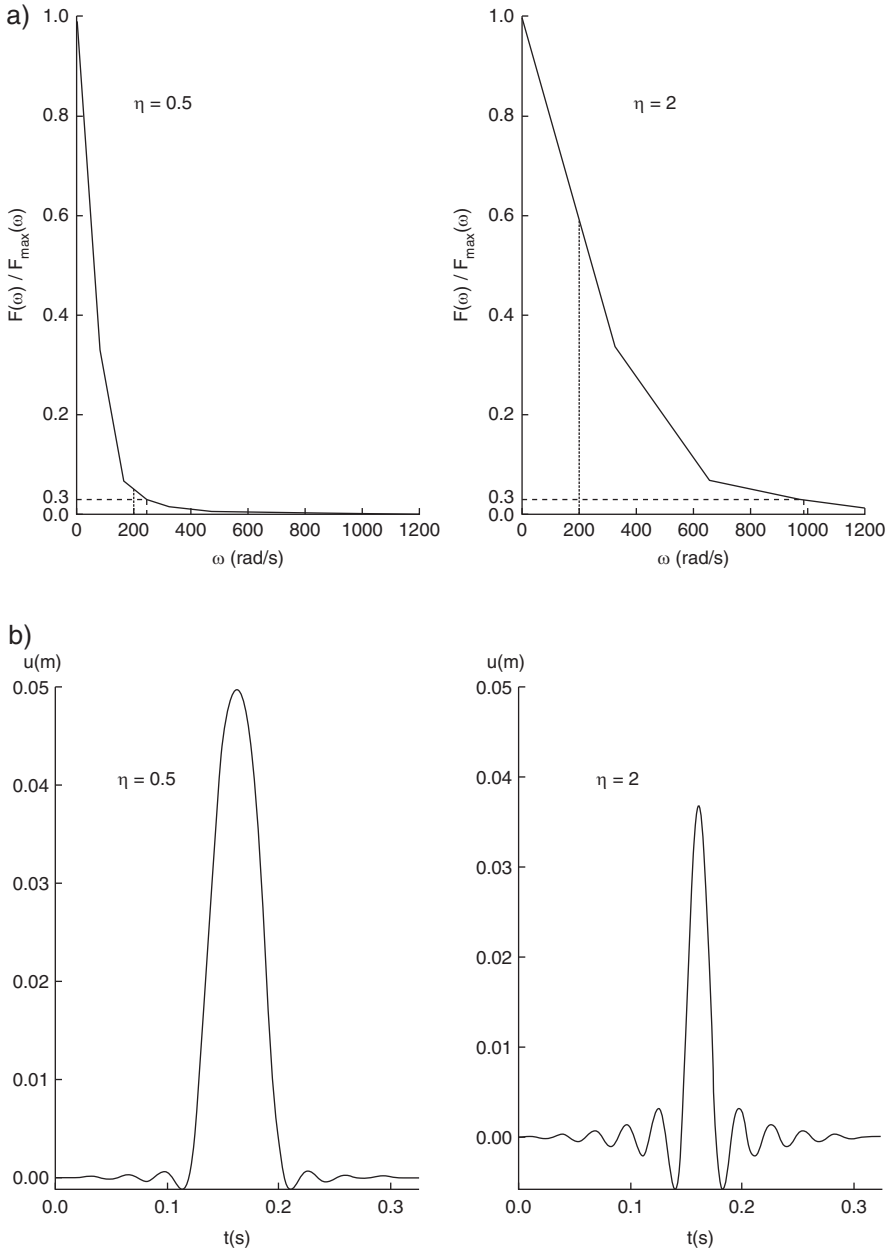

Figure 2. (a) Normalized one-side frequency response: $\eta = 0.5$ (left), $\eta = 2$ (right); (b) filtered pulse: $\eta = 0.5$ (left), $\eta = 2$ (right).

pulse, η. For that reason, we chose a rectangular soil box with dimensions $L_m = 10 \cdot a$ and $H_s = L_m/2 = 5 \cdot a$ (Fig. 1). Also, for merely practically reasons, the maximum number of space intervals in the grid in the horizontal (x) direction is set at 250 and in the vertical (y) direction at 400 (125 in the soil box and 275 in the building). The minimum spatial interval for this setup is $\Delta x_{\min} = L_m/250 = 95.5/250 = 0.382$ m. For a finer grid, the computational time increases rapidly. Having this limitation in mind, from Eq. (3) and for $\eta = 2$ ($\omega_{\max} = 980$ rad/s), the shortest wavelength is $\lambda_{\min} = 1.603$ m, and the finest grid density for this wavelength is $m = \lambda_{\min}/\Delta x_{\min} = 1.603/0.382 \approx 4$ points/$\lambda_{\min} < m_{\min}$.

Our numerical scheme is $O\left(\Delta t^2, \Delta x^2\right)$, so from the above recommendations we should have at least $m = 12$ points/$\lambda_{\min}$ to resolve for the shortest wavelength, $\lambda_{\min}$. This implies that the pulse should be low-pass filtered. A cut-off frequency $\omega_c = 200$ rad/s was chosen, and the pulse was low-pass filtered (Fig. 2b). This implies that $\lambda_{\min} = 7.854$ m and then the grid density is

$$m = \frac{\lambda_{\min}}{\Delta x_{\min}} = \frac{7.854}{0.382} \approx 20 \text{ points}/\lambda_{\min} > m_{\min}. \tag{4}$$

It can be seen in Fig. 2a (dotted lines) that for $\eta = 0.5$ only a negligible amount of the total power is filtered out, while for $\eta = 2$ a considerable amount is filtered out. Also, it can be seen in Fig. 2b that for $\eta = 2$ the amplitude of the filtered pulse is smaller than the amplitude of the non-filtered pulse, which is $A = 0.05$ m, while for $\eta = 0.5$ the amplitude is almost equal with the amplitude of the non-filtered pulse. From numerical tests, it has been shown that the viscous absorbing boundary rotated toward the centre of the foundation reflects only a negligible amount of energy back into the model (Gicev, 2005).

For 2-D problems, the numerical scheme is stable if the time increment (Mitchell, 1969) is:

$$\Delta t \leq \min\left(\frac{1}{\beta\sqrt{\frac{1}{\Delta x^2} + \frac{1}{\Delta y^2}}}\right). \tag{5}$$

Further, we assume that the shear stress in the x direction depends only upon the shear strain in the same direction and is independent of the shear strain in the y direction (and vice versa for shear stress in the y direction). The motivation for this assumption comes from our simplified representation of layered soil, which is created by deposition (floods and wind) into more or less horizontal layers. The soil is assumed to be ideally elastoplastic, and the constitutive $\sigma - \varepsilon$ diagram is shown in Fig. 3. Further, it is assumed that the contacts remain bonded during the analysis and the contact cells C, D, E, F, G, and H in Fig. 4 remain linear, as does the zone next to the artificial boundary (the bottom four rows and the left-most and right-most four columns).

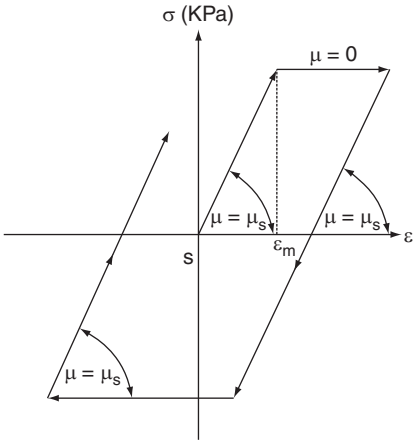

Figure 3. The constitutive law, $\sigma - \varepsilon$, for the soil.

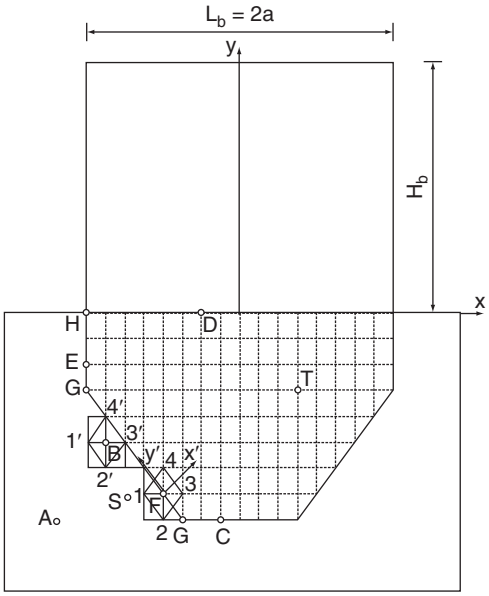

Figure 4. Numerical model with nonlinear soil. The points A, S, B, 1, 2, 1′, and 2′ can undergo permanent strains.

For our problem, the system of three partial differential equations (for u, v, and w) describing the dynamic equilibrium of an elastic body is reduced to the third equation only (because $u = v = \frac{\partial}{\partial z} = 0$). Neglecting the body forces in the z direction ($F_z = 0$), this equation is:

$$\rho \frac{\partial^2 w}{\partial t^2} = \left(\frac{\partial \tau_{xz}}{\partial x} + \frac{\partial \tau_{yz}}{\partial y} \right). \tag{6}$$

Introducing the new variables $v = \partial w/\partial t$, $\varepsilon_{xz} = \partial w/\partial x$, and $\varepsilon_{yz} = \partial w/\partial y$, and dividing (5) by ρ, the order of (6) is reduced to the system of three first-order partial differential equations (PDE)

$$\underline{U}_{,t} = \underline{F}_{,x} + \underline{G}_{,y}, \tag{7}$$

where

$$\underline{U} = \begin{Bmatrix} v \\ \varepsilon_{xz} \\ \varepsilon_{yz} \end{Bmatrix}, \quad \underline{F} = \underline{F}(\underline{U}) = \begin{Bmatrix} \frac{1}{\rho}\tau_{xz} \\ v \\ 0 \end{Bmatrix}, \quad \underline{G} = \underline{G}(\underline{U}) = \begin{Bmatrix} \frac{1}{\rho}\tau_{yz} \\ 0 \\ v \end{Bmatrix}. \tag{8}$$

The first equation in (7) represents the dynamic equilibrium of forces in the z direction with neglected body force F_z, while the second and third equations give the relations between the strains and the velocity. The abbreviations $\varepsilon_x = \varepsilon_{xz}$, $\sigma_x = \tau_{xz}$, $\varepsilon_y = \varepsilon_{yz}$, and $\sigma_y = \tau_{yz}$ are used later in the text. The Lax–Wendroff computational scheme (Lax and Wendroff, 1964) is used for solving Eq. (7) (Gicev, 2005).

3. Energy and Permanent Strain Distribution

As a test example, the properties of the Holiday Inn hotel in Van Nuys, California in the east–west direction are considered (Blume and Assoc., 1973). A question arises about how to choose the yielding strain ε_m (Fig. 3) to study permanent strain distribution. The displacement, the velocity, and the linear strain in the soil ($\beta_s = 250$ m/s) during the passage of a plane wave in the form of a half-sine pulse are:

$$w = A \sin\left[\frac{\pi}{t_{d0}}\left(t - \frac{s}{\beta_s}\right)\right], \tag{9}$$

$$v = \dot{w} = \frac{\pi}{t_{d0}} A \cos\frac{\pi t}{t_{d0}}, \tag{10}$$

$$|\varepsilon| = \frac{v_{\max}}{\beta_s} = \frac{\pi A}{\beta_s t_{d0}}. \tag{11}$$

If, for a given input plane wave, we choose the yielding strain ε_m given by (11) multiplied by some constant between 1 and 2, the strains in both directions will remain linear before the wave reaches the free surface or the foundation. This case can be called "intermediate nonlinearity". If we want to analyze only the nonlinearity due to scattering and radiating from the foundation, we should avoid the occurrence of the nonlinear

strains caused by reflection from the half-space boundary. Then we may choose $\varepsilon_m = \max(2\pi A \sin\gamma/\beta_s t_{d0}; 2\pi A \cos\gamma/\beta_s t_{d0})$. We call this case "small nonlinearity".

If the soil is allowed to undergo permanent strains only due to wave passage of incident waves in the full space, then we may choose the maximum strain $\varepsilon_m < \max(\pi A \sin\gamma/\beta_s t_{d0}; \pi A \cos\gamma/\beta_s t_{d0})$. This condition guarantees that in either the x or y direction the soil will undergo permanent strains during the passage of the plane wave. Generally, the yielding strain can be written as

$$\varepsilon_m = C\frac{v_{\max}}{\beta_s} = C\frac{\pi A}{\beta_s t_{d0}}, \tag{12}$$

where C is a constant that controls the yielding stress (strain) in the soil. We then consider the following cases of nonlinearity, depending upon C:

1. $\boldsymbol{C \geq 2}$**: Small nonlinearity**. Permanent strain does not occur until the wave hits the foundation with any angle of incidence.
2. $\boldsymbol{1 \leq C < 2}$**: Intermediate nonlinearity**. Permanent strain does not occur until the wave is reflected from the free surface or is scattered from the foundation, for any angle of incidence. Permanent strain will or will not occur after the reflection of the incident wave from the free surface, depending upon the angle of incidence.
3. $\boldsymbol{C < 1}$**: Large nonlinearity**. Permanent strain occurs after reflection from the free surface. Permanent strain may or may not occur before the wave reflects from the foundation surface, depending upon the angle of incidence.

4. Energy Distribution in the System

The energy flow through a given area can be defined, in terms of a plane-wave approximation (Aki and Richards, 1980), as:

$$E_{in}^{a} = \rho_s \cdot \beta_s \cdot A_{sn} \int_0^{t_{d0}} v^2 \cdot dt, \tag{13}$$

where ρ_s and β_s are density and shear-wave velocity in the soil and v is a particle velocity, which, for the excitation considered in this paper, is given by Eq. (10). A_{sn} is the normal area through which the wave is passing. For our geometrical settings of the soil (Fig. 1), the area normal to the wave passage is:

$$A_{sn} = 2 \cdot H_s \cdot \sin\gamma + L_m \cdot \cos\gamma = L_m \cdot (\sin\gamma + \cos\gamma). \tag{14}$$

Inserting Eqs. (10) and (14) into (13) and integrating, the analytical solution for the input wave energy into the model is

$$E_{\text{in}}^{a} = \rho_s \cdot \beta_s \cdot L_m \cdot (\sin\gamma + \cos\gamma) \cdot \left(\frac{\pi \cdot A}{t_{d0}}\right)^2 \cdot \frac{t_{d0}}{2}. \tag{15}$$

As can be seen from Eq. (15), for the defined size of the soil island, L_m, and the defined angle of incidence, γ, the input energy is reciprocal with the duration of the pulse and is a linear function of the dimensionless frequency η (Eq. (1a)). Because the short pulses are low-pass filtered up to $\omega_c = 200$ rad/s (Fig. 2b), the analytical and the numerical solutions (13) for input wave energy do not coincide (Fig. 5). Since our system is conservative, the input energy is balanced by:

- Cumulative energy going out from the model, E_{out}, computed using Eq. (13); cumulative hysteretic energy (energy spent for creation and development of permanent strains in the soil), computed from:

$$E_{\text{hys}} = \sum_{t=0}^{T_{\text{end}}} \Delta t \cdot \sum_{i=1}^{N} \left(\sigma_{xi}(\Delta\varepsilon_{xpi} + 0.5 \cdot \Delta\varepsilon_{xei}) + \sigma_{yi}(\Delta\varepsilon_{ypi} + 0.5 \cdot \Delta\varepsilon_{yei})\right), \tag{16}$$

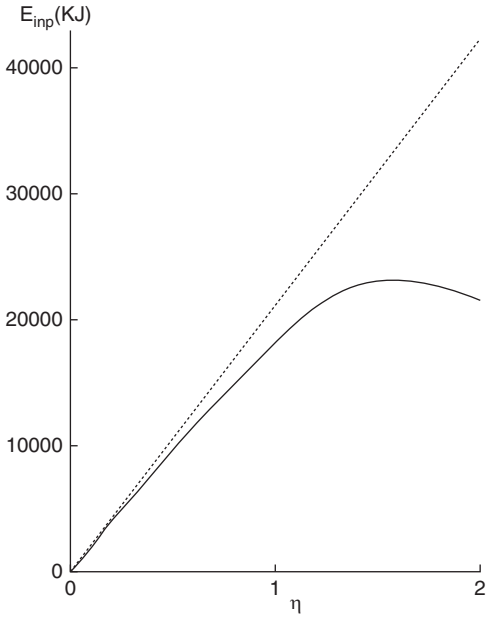

Figure 5. Input energy in the model: from analytic half-sine pulse (dashed line); from low-pass filtered half-sine pulse (solid line).

where N is the total number of soil points; σ_{xi}, σ_{yi} are the stresses at the point i in the x and y directions, respectively; $\Delta\varepsilon_{xpi} = \varepsilon_{xpi}^{t+\Delta t} - \varepsilon_{xpi}^{t}$ is the increment of the permanent strain in the x direction at point i; and $\Delta\varepsilon_{ypi} = \varepsilon_{ypi}^{t+\Delta t} - \varepsilon_{ypi}^{t}$ is the increment of the permanent strain in the y direction at point i

- Instantaneous energy in the building, consisting of kinetic and potential energy, which can be computed from:

$$E_b = E_k + E_p = 0.5 \cdot \Delta x \cdot \Delta y_b \cdot \sum_{i=1}^{N} \left(\rho \cdot v_i^2 + \mu \cdot (\varepsilon_x^2 + \varepsilon_y^2)\right). \qquad (17)$$

In Fig. 6, this balance is shown for a pulse with $\eta = 1.5$, for incident angle $\gamma = 30°$, and a yielding strain defined by $C = 1.5$ (Eq. (12)).

To study the effect of scattering from the foundation only, the building is considered to be high enough so that the reflected wave from the top of the building cannot reach the building-foundation contact during the analysis. The analysis is terminated when the wave completely exits the soil island. In this study, the hysteretic energy in the soil and the energy in the building are the subjects of interest. In Fig. 7, these two types of energy are presented as

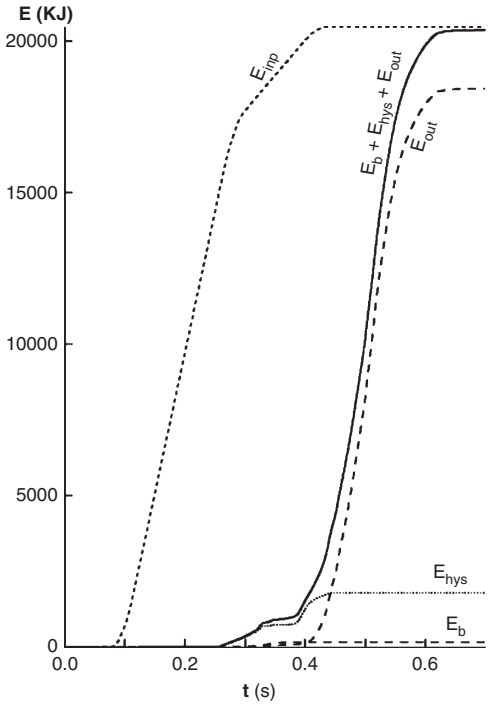

Figure 6. Energy balance in the model for $\gamma = 30°$ and $\eta = 1.5$.

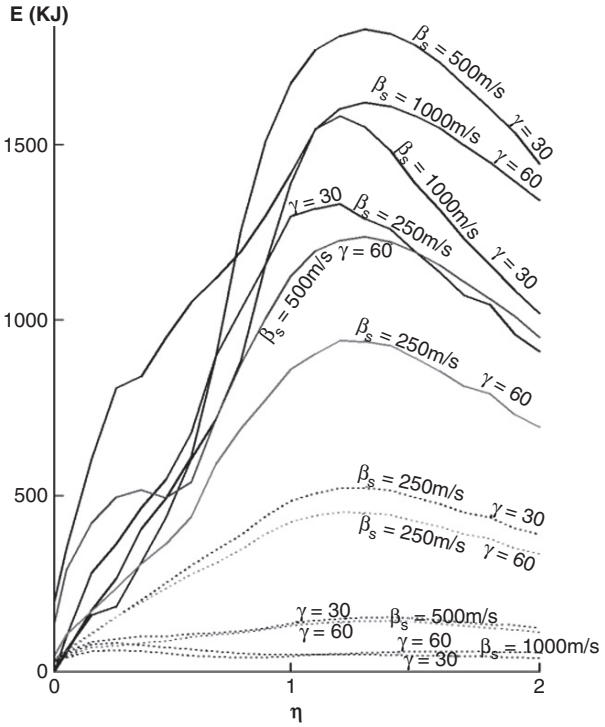

Figure 7. Hysteretic energy (solid lines) and energy entering the building (dashed lines) vs. dimensionless frequency for intermediate nonlinearity $C = 1.5$.

functions of the dimensionless frequency η. Considering the energy entering the building (dashed lines), the results confirm the expectations that as the foundation becomes stiffer, a larger part of the input energy is scattered and less energy enters the building. In contrast, the results for hysteretic energy in the soil are not so straightforward. For an angle of incidence $\gamma = 60°$, the results are as would be expected—e.g., the hysteretic energy increases as the foundation stiffness increases. However, this is not the case for the angle of incidence $\gamma = 30°$. It can be seen that at some frequency intervals the hysteretic energy can be larger for softer foundations. For example, for $\eta \leq 0.7$ and an angle of incidence $\gamma = 30°$, as the foundation becomes softer the hysteretic energy becomes larger (the softest foundation we considered had $\beta_f = 250$ m/s). Similarly, a foundation with medium stiffness, $\beta_f = 500$ m/s, for $\eta > 0.8$ and an angle of incidence $\gamma = 30°$, causes the largest hysteretic energy in the soil, where the maximum occurs at $\eta = 1.5$. This unexpected behaviour of the soil can be explained by the destructive interference that may occur with stiffer foundations, which decreases the released hysteretic energy in the soil.

5. Distribution of the Permanent Strain in the Soil

Considering Fig. 8, and starting from dynamic equilibrium of the differential pentahedron shown in the figure, we can find the principal stress at a point and its direction as:

$$\tau_{zp} = \tau_{zx} \cos\gamma + \tau_{zy} \sin\gamma \quad \text{and} \quad \gamma = \tan^{-1} \frac{\tau_{zy}}{\tau_{zx}}.$$

The principal permanent strain in the soil is illustrated in Fig. 9a, b, c, for the case of small nonlinearity ($C = \sqrt{3}$) for two angles of incidence, $\theta = 30°$ and $60°$, and for three foundation stiffnesses, $\beta_f = 2500$, 500, and 1000 m/s. This value of C guarantees that for angles of incidence $30° \leq \gamma \leq 60°$ there is no occurrence of permanent strain until the wave hits the foundation.

The principal permanent strain is illustrated in Fig. 10a, b, c, for the case of intermediate nonlinearity ($C = 1.5$) for the same angles of incidence, $\theta = 30°$ and $\theta = 60°$ and for three foundation stiffnesses, $\beta_f = 250$, 500, and 1000 m/s. In this case, permanent strain occurs before the wave hits the foundation but after it reflects from the free surface.

For long pulses $\eta = 0.1$, it can be seen from Fig. 9a that for an angle of incidence $\gamma = 30°$ there is a small, permanent strain for the stiffest foundation ($\beta_f = 1000$ m/s) only, while for softer foundations the soil remains linear after the pulse has left the model. For intermediate nonlinearity, shown in Fig. 10a, for an angle of incidence $\gamma = 30°$ it can be seen that after the creation of nonlinear zones the effect of the interaction is negligible compared with the effects of interference of the incoming wave and the reflected wave from the

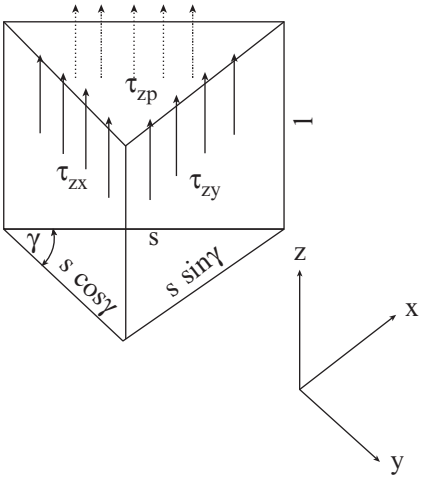

Figure 8. Orthogonal and principal shear stresses on differential pentahedron.

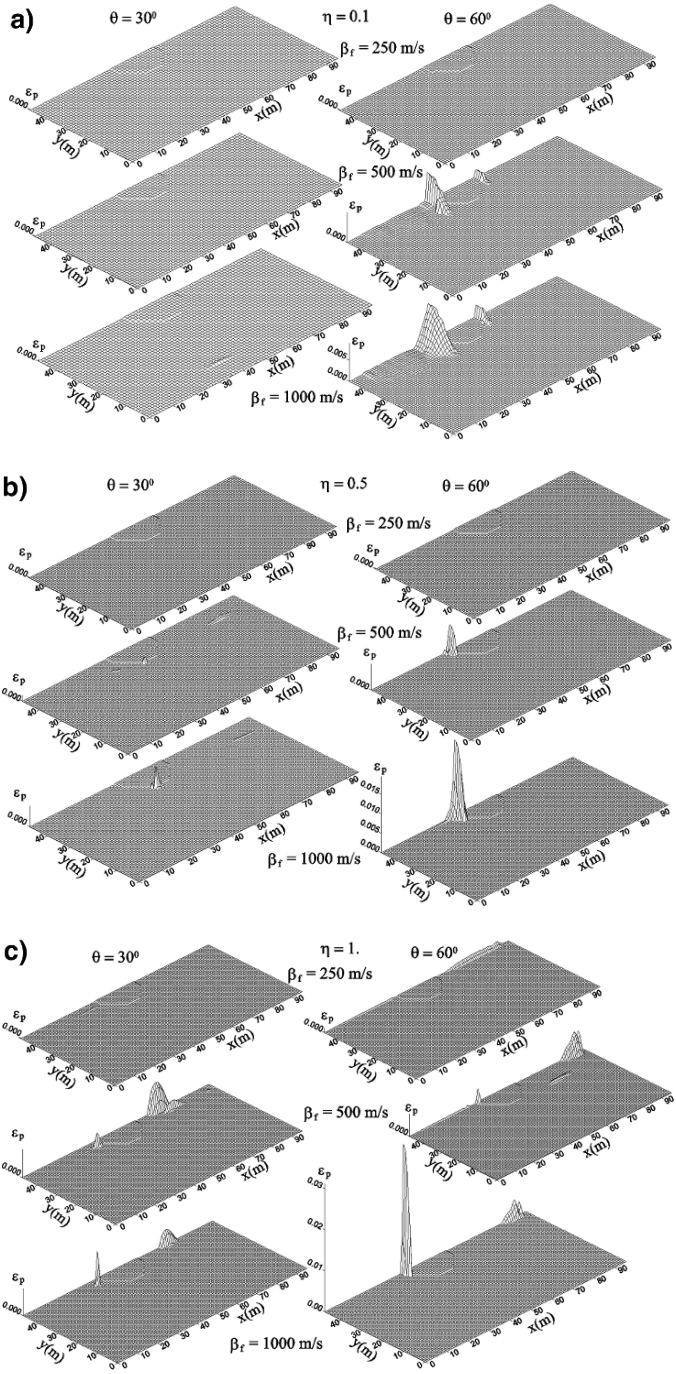

Figure 9. Principal permanent strain in the soil for: (a) $\eta = 0.1$; (b) $\eta = 0.5$; (c) $\eta = 1$, two angles of incidence, and three foundation stiffness. Small nonlinearity in the soil $C = 1.73$.

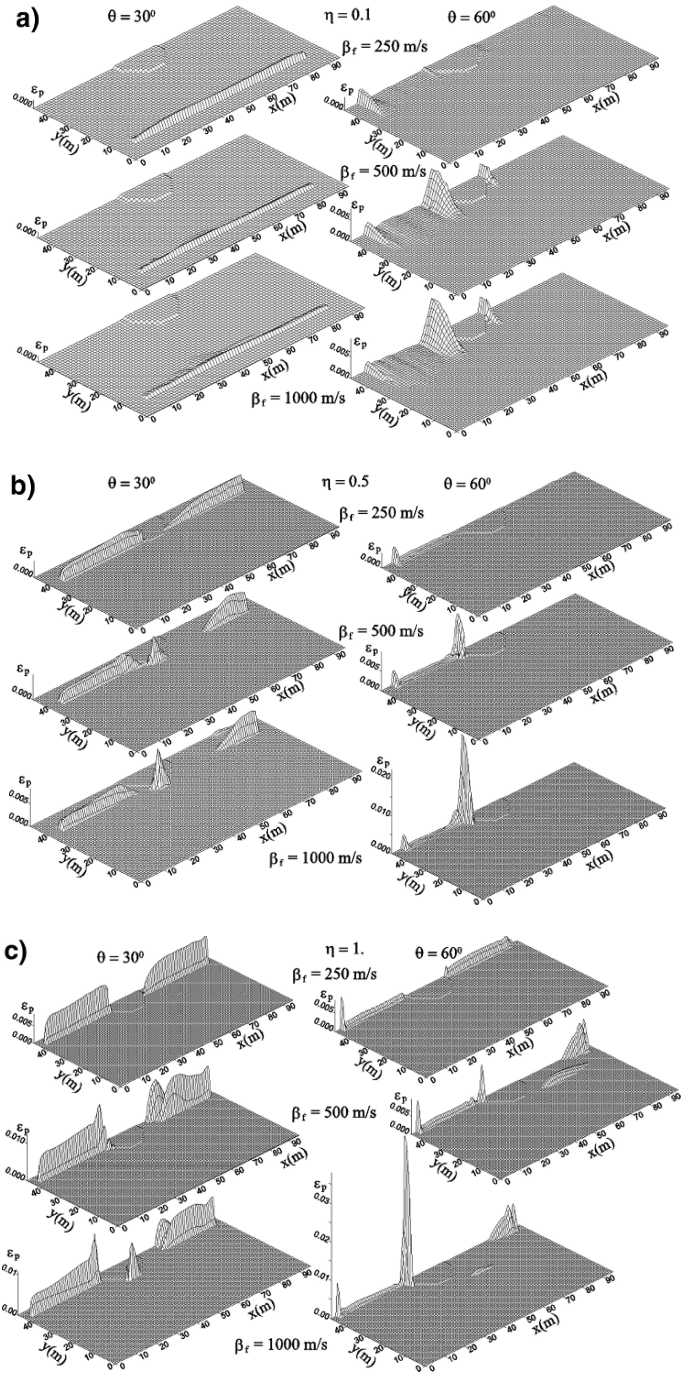

Figure 10. Principal permanent strain in the soil for: (a) $\eta = 0.1$; (b) $\eta = 0.5$; (c) $\eta = 1$, two angles of incidence, and three foundation stiffness. Small nonlinearity in the soil $C = 1.5$.

free surface. This is not the case for $\gamma = 60°$. It can be concluded from Figs. 9a and 10a that for stiffer foundations the effect of interaction is more dominant than the effect of the interference. For the softest considered foundation, the effect of the interaction on creation of nonlinear strains is small.

The observations are similar for a five-times-shorter pulse $\eta = 0.5$. It can be seen from Figs. 9b and 10b that for the softest foundation the effect of the interaction is negligible and that as the foundation becomes stiffer the nonlinear zones are created and developed in the soil next to the front of the foundation.

As the pulse becomes shorter, $\eta = 1$, it can be seen that nonlinear zones are also formed behind the foundation. This can be explained by the interference of waves reflected from the free surface and diffracted around the foundation. Again, the permanent strain in front of the foundation increases as the stiffness of the foundation increases.

6. Conclusions

Numerical methods are powerful tools for studying nonlinear soil-structure interaction problems. Because of grid dispersion, the selection of the grid spacing must be done carefully. Short waves cannot be reconstructed even with very fine grids, and the incident wave (pulse) should be low-pass filtered to utilize numerical methods effectively.

In the presence of a foundation and small angles of incidence (close to vertical incidence), the permanent strains in the y direction are dominant, while for large angles of incidence (close to horizontal incidence) the permanent strains in the x direction are dominant.

For long waves and small angles of incidence (Figs. 9a and 10a for $\theta = 30°$, the effect of the interaction on the nonlinear response in the soil is small. For soft foundations, $\beta_f = 250$ m/s, and small incident angles (the top left plots in Figs. 9a, b, c and 10a, b, c), the effect of the interaction on the nonlinear response of the soil is also small. As the foundation becomes stiffer, zones of large permanent strains develop around the foundation. For stiff foundations, short waves ($\eta = 1$ and $\eta = 2$, and large incidence angles, a zone of permanent strains develops behind the foundation, which appears to be due to the concentration of rays associated with diffraction of the waves from the foundation. The zones of large permanent strains illustrated in Figs. 9a, b, c and 10a, b, c are responsible for the damage and failures in the shallow infrastructure (water and gas pipes, underground cables, etc.) that accompany large earthquakes and cause interruptions of gas and water supplies (Trifunac and Todorovska, 1997, 1998a, 1998b).

As the large and permanent strains develop along the foundation-soil interface, the effective foundation compliances are reduced, which decreases the equivalent rocking stiffness of the foundation-structure system. With simultaneous action of in-plane wave motions, which are always present in 3-D settings during earthquake excitation and which will excite the in-plane rocking of the model we studied in this paper, it is easy to see how the nonlinear zones in the soil (as illustrated in Figs. 9 and 10) will take the structure one step closer to overturning or even eventual collapse, as in the examples mentioned in the introduction.

References

Abdel-Ghaffar, A. M. and Trifunac, M. D. (1977) Antiplane dynamic soil–bridge interaction for incident plane SH-waves. In *Proc. 6th World Conf. Earthquake Eng.*, Vol. 2, New Delhi, India.

Aki, K. and Richards, P. (1980) *Quantitative Seismology, Theory and Methods*, San Francisco, W. H. Freeman & Co.

Alford, R. M., Kelly, K. R., and Boore, D. M. (1974) Accuracy of finite-difference modeling of the acoustic wave equation, *Geophysics* **39**, 834–842.

Alterman, Z. and Karal, F. C. (1968) Propagation of elastic waves in layered media by finite difference methods, *Bull. Seism. Soc. of Am.* **58**(1), 367–398.

Aviles, J., Suarez, M., and Sanchez-Sesma, F. J. (2002). Effects of wave passage on the relevant dynamic properties of structures with flexible foundation, *Earthq. Eng. Struct. Dynam.* **31**, 139–159.

Blume J. A. and Assoc. (1973) Holiday Inn. In L. M. Murphy (ed.), *San Fernando, California, Earthquake of February 9, 1971*, U.S. Dept. of Commerce, National Oceanic and Atmospheric Administration, Washington, D.C., pp. 359–394.

Boore, D. M. (1972) Finite difference methods for seismic wave propagation in heterogeneous materials. In B. A. Bolt (ed.), *Seismology, Surface Waves and Earth Oscillations*, Vol. 11 of *Methods in Comp. Physics*, New York, pp. 1–37, Academic Press.

Dablain, M. A. (1986) The application of high-order differencing to the scalar wave equation, *Geophysics* **51**(1), 54–66.

Fah, D. J. (1992) A hybrid technique for the estimation of strong ground motion in sedimentary basins, Ph.D. Dissertation, Swiss Federal Institute of Technology, Zurich, Switzerland.

Gicev, V. (2005) Investigation of soil-flexible foundation–structure interaction for incident plane SH waves, Ph.D. Dissertation, Dept. of Civil Engineering, Univ. Southern California, Los Angeles, California.

Hayir, A., Todorovska, M. I., and Trifunac, M. D. (2001) Antiplane response of a dike with flexible soil-structure interface to incident SH waves, *Soil Dynam. Earthq. Eng.* **21**, 603–613.

Lax, P. D. and Wendroff, B. (1964) Difference schemes for hyperbolic equations with high order of accuracy, *Comm. Pure Appl. Math.* **XVII**, 381–398.

Lee, V. W. (1979) Investigation of three-dimensional soil-structure interaction, Report No. CE 79-11, Dept. of Civil Engineering, Univ. of Southern California, Los Angeles, CA.

Luco, J. E. and Wong, H. L. (1977) Dynamic response of rectangular foundations for Rayleigh wave excitation. In *Proc. 6th World Conf. Earthq. Eng.*, Vol. 2, New Delhi, India.

Mitchell, A. R. (1969) *Computational Methods in Partial Differential Equations*, New York, Willey.

Moczo, P. (1989) Finite-difference technique for SH-waves in 2-D media using irregular grids—application to the seismic response problem, *Geophys. J. Int.* **99**, 321–329.

Seed, H. B. (1970) Soil problems and soil behavior. In R. L. Wiegel (ed.), *Earthquake Engineering*, Englewood Cliffs, N.J., Prentice Hall, pp. 227–251.

Todorovska, M. I., Hayir, A., and Trifunac, M. D. (2001) Antiplane response of a dike on flexible embedded foundation to incident SH-waves, *Soil Dynam. Earthq. Eng.* **21**, 593–601.

Trifunac, M. D. (1972) Interaction of a shear wall with the soil for incident plane SH waves, *Bull. Seism. Soc. Am.* **62**(1), 63–83.

Trifunac, M. D. (1995) Empirical criteria for liquefaction in sands via standard penetration tests and seismic wave energy, *Soil Dynam. Earthq. Eng.* **14**(6), 419–426.

Trifunac, M. D. and Todorovska, M. I. (1997) Northridge, California, earthquake of 17 January 1994: Density of pipe breaks and surface strains, *Soil Dynam. Earthq. Eng.* **16**(3), 193–207.

Trifunac, M. D. and Todorovska, M. I. (1998a) Nonlinear soil response as a natural passive isolation mechanism—the 1994 Northridge, California earthquake, *Soil Dynam. Earthq. Eng.* **17**(1), 41–51.

Trifunac, M. D. and Todorovska, M. I. (1998b) The Northridge, California, earthquake of 1994: Fire ignition by strong shaking, *Soil Dynam. Earthq. Eng.* **17**(3), 165–175.

Tsynkov, S. V. (1998) Numerical solution of problems on unbounded domains: A review, *Appl. Numerical Math.* **27**, 465–532.

Westermo, B. D. and Wong, H. L. (1977) On the fundamental differences of three basic soil-structure interaction models, *Proc. 6th World Conf. of Earth. Eng.*, Vol. 2, New Delhi, India.

Wong, H. L. and Trifunac, M. D. (1974) Interaction of a shear wall with the soil for incident plane SH waves: Elliptical rigid foundation, *Bull. Seism. Soc. Am.* **64**(6), 1825–1884.

Wong, H. L. and Trifunac, M. D. (1975) Two-dimensional antiplane, building-soil–building interaction for two or more buildings and for incident plane SH waves, *Bull. Seism. Soc. Am.* **65**(6), 1863–1885.

Zahradnik, J., Moczo, P., and Hron, F. (1993) Testing four elastic finite-difference schemes for behaviour at discontinuities, *Bull. Seism. Soc. Am.* **83**, 107–129.